Investigation of Bulge Radius Variation and its Effect on the Flow Stress in the Hydraulic Bulge Test

Lucian LĂZĂRESCU, Dan-Sorin COMŞA, Ioan NICODIM, Ioan CIOBANU and Dorel BANABIC

[1)] CERTETA Research Centre, Technical University of Cluj-Napoca, Cluj-Napoca Romania, lucian.lazarescu@tcm.utcluj.ro

Abstract. The assumption of the spherical shape of the bulge is the theoretical basis of the bulge test with circular die. In this paper the deviation of the meridian profile from the corresponding circle shape is investigated using the Least Square Circle Fitting of the experimental data. The residuals were determined for different bulge height. The effect of two procedural parameters in the ARAMIS software (the radius defining the circular area for the calculation of bulge radius, and the radius for the calculation of average thickness, respectively) on the amount of bulge radius as well as on the flow stress curve has been investigated. Finally a procedure for the determination the ratio between the two procedural parameters is presented.

Keywords: Hydraulic bulge test, Flow stress, Bulge radius variation

1. INTRODUCTION

The hydraulic bulge test is one of the most used methods for the determination of stress-strain curve in biaxial stress state conditions. One of the advantages of the hydraulic bulge test is the absence of contact between the specimen surface and the tools (and therefore the absence of friction) in the area of interest, leading to a simplification of the analytical solutions for the calculation of biaxial stress and biaxial strain.

One of the main assumptions is that the shape of the bulge is spherical, and therefore the bulge radius is the same in any meridian section. The bulge shape has been investigated by other authors with many years ago such as Ranta-Eskola [1], who examined the effect of the geometry of the bulge and the measuring procedure on biaxial stress-strain curves. Atkinson [2] and Banabic [3] extended an earlier solution for polar strain to derive the effective radius of curvature near the pole and generates an accurate explicit expression for the calculation of membrane stress at the pole. The authors of some recently published papers [4], [5], [6], [7] deal with the development of procedures for the validation of the biaxial stress-strain curves from the bulge test. Lemoine [8] investigated the limitations of membrane theory in the hydraulic bulge test.

In this paper the deviations of the bulge profile from the assumed circular shape is investigated by Least Square Circle Fitting of the experimental data at different bulge heights. The effect of two procedural parameters on the bulge radius as well as on the flow stress curve is determined.

2. EXPERIMENTS

2.1. Experimental setup

Figure 1 shows a general view on the experimental set-up used to perform the hydraulic bulge tests. This consists in three units: 1) a hydraulic device for pressure development; 2) a bulging device containing the die; 3) - a 3D optical measurement system ARAMIS.

An insert die with an aperture diameter of 80 mm and a fillet radius of 5 mm was used to perform the bulge experiments. A DC04 steel sheet having the nominal thickness of 0.85 was chosen for the experiments.

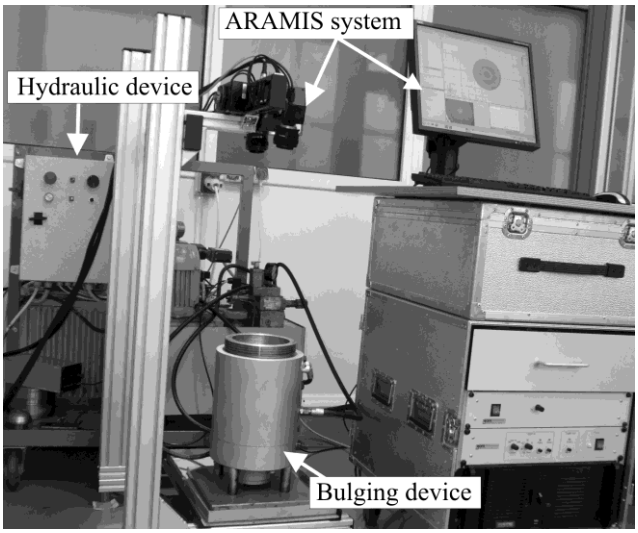

Figure 1. Experimental setup for hydraulic bulge test.

2.2. Determination of biaxial stress-biaxial strain curve

By assuming the material isotropy and the spherical shape of the bulged specimen, the biaxial stress can be calculated using the Laplace's equation

$$\sigma_b = \frac{p\rho}{2t} \tag{1}$$

where p is the internal pressure; ρ is the bulge radius and t is the average current thickness near the pole.

The biaxial stress given by Eq. (1) can be calculated on the basis of the three variables: the internal pressure is continuously recorded during the experiment using a pressure gauge; the bulge radius and the average thickness are determined using the ARAMIS system on the basis of photogrammetry.

By assuming that the material is incompressible, the biaxial strain (ε_b) can be calculated using the equation

$$\varepsilon_b = \ln\left(\frac{t}{t_0}\right) \tag{2}$$

where t_0 is the original sheet thickness.

During the procedure for the determination the flow stress curve using the ARAMIS software it is necessary to choice the two radii related to the bulge surface. First is the radius R_1 defining the circular area for the best sphere fitting of the specimen shape and for bulge radius calculation (Fig. 2). The second radius R_2 is introduced to define the circular area for the average thickness calculation.

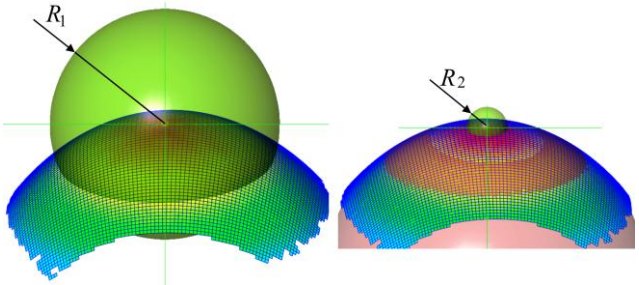

Figure 2. The bulge shape and the two procedural parameters (R_1) and (R_2).

In the literature there is not a clear specification for the choice of the two radii. Lemoine [8] suggests that the radius R_1 should be sufficiently large, while the radius R_2 may be fairly small.

3. RESULTS

3.1. Evaluation of meridian profile of specimen

The bulge geometries were determined using the ARAMIS system, and then the bulge shape was sectioned using a meridian plane containing the bulge axe of symmetry and the meridian profile was obtained. In order to evaluate the shape of bulge profile, the Least Squares Circle Fit was used and the best circle by minimizing the residuals through the least square approximation was determined. Two statistical parameters are used in order to asses the difference between the experimental profile and the best circle fit. These are the residual (e), defining the difference between experimental data (y) and calculated value (y')

$$e = y - y', \tag{3}$$

and the standard error of estimate (SEE), showing the square root of the residuals variance

$$SEE = \sqrt{\frac{\sum (y_i - y_i')^2}{q-2}} \tag{4}$$

where q is the number of experimental data.

Figure 3 shows the difference between experimental points of meridian profile of specimen and the points of fitted circle (residuals) for bulge height of 10, 25, 30 and 32 mm, respectively. While at dome height up to 25 mm the residuals are very close to zero, they are larger at dome height over 25 mm. The residuals are approximately symmetrical distributed around the bulge axis (x = 0). At the bulge height over 25 mm, the residuals are positive near the dome apex (x = ± 10 mm), and near the edge of specimen (x > ± 26 mm), and negative otherwise. From **Figure 3** one may also notice that the residuals are higher near the edges of the specimen (x = ± 30 mm), but the maximum value is under 0.4 mm.

Figure 4 shows variations in SEE with radius for circle fit of specimen profile (R_1) and bulge height. As shown in **Figure 4**, the effect of radius R_1 on the SEE becomes significant only at large values of bulge height. As one may notice, in this case, the SEE increases when the radius R_1 increases.

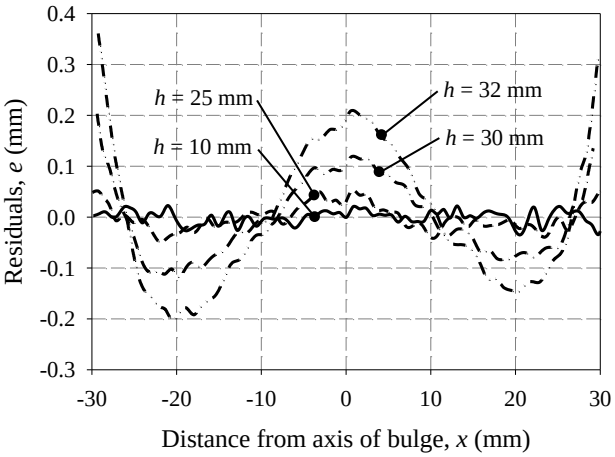

Figure 3. Residuals showing the difference between experimental meridian profile of specimen and the fitted circle

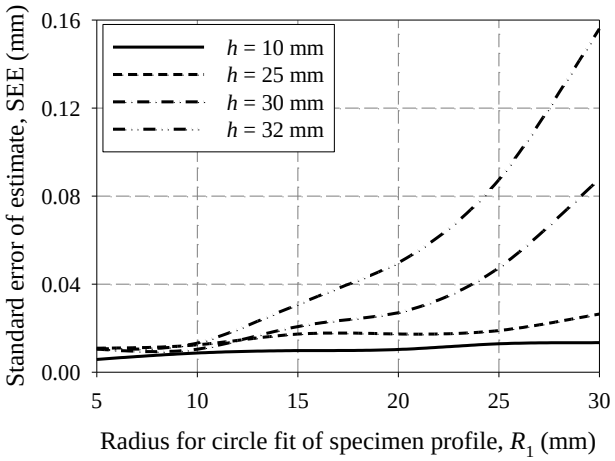

Figure 4. Effect of radius (R_1) on SEE.

Figure 5 shows the effect of bulge height on SEE for radius (R_1) of 10, 20, 25 and 30 mm, respectively. From Figure 1, it is evident that for R_1 = 10 mm the SEE remain close to zero up the end of bulge experiment. At radii (R_1) over 20 mm, the SEE remain close to zero only up to the bulge height of about 23 mm. After this value of bulge height, the SEE increases as the bulge height increases. This increase

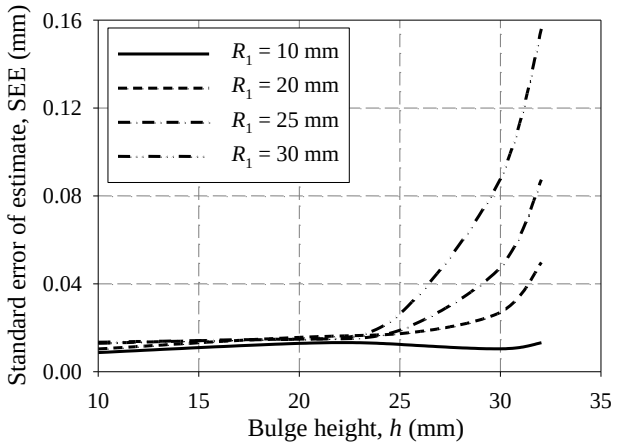

Figure 5. Relationship between the SEE and bulge height.

The residuals from **Figure 3** and SSE seen in **Figures 4** and **5** indicate that the meridian profile o specimen deviates from its original circle shape only when bulge height is larger than 25 mm.

3.2. Bulge radius deviation

The bulge radius was calculated using ARAMIS software for samples heaving the bulge height of 20, 25, 30 and 32 mm, respectively and for radius R_1 of 10, 20, 25 and 30 mm, respectively. **Figure 6** shows the variations in bulge radius with h and R_1. It is seen that the bulge radius is very sensitive to the change in R_1, especially when the bulge height is larger than 25 mm. For a bulge height of 32 mm, as the radius R_1 increase from 10 to 30 mm, the bulge radius increases from 34.94 to 40.36 mm. Therefore, the bulge radius was increased with 5.41 mm, by an increase in the radius R_1 from 10 to 30 mm.

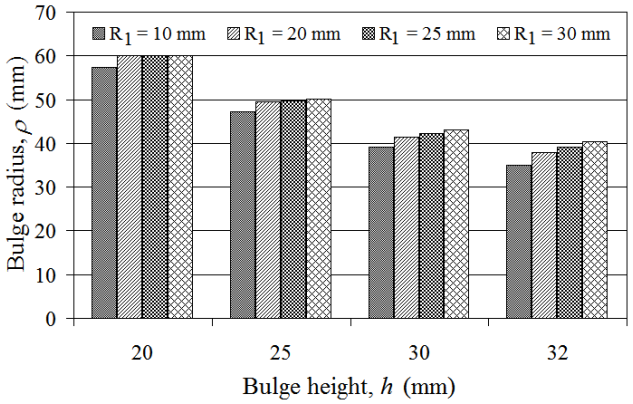

Figure 6. Relationship between the bulge radius and bulge height for different radii (R_1).

3.3. Effect of R_1 and R_2 radii on stress-strain curve

Figure 7 shows the influence of the radius R_1 on the biaxial stress - biaxial strain curve shape. These curves were obtained from experiments, while the radius R_2 was kept constant at 5 mm. As shown in Figure 5, when the radius (R_1) increases from 10 to 30 mm, the biaxial stress increases, and the σ_b-ε_b curves, tend to move upwards (in direction of the arrow) to higher values of biaxial stress. The increase of biaxial stress with the increase in radius R_1 may be explained by the reason that the bulge radius also increases as the radius R_1 increases, as discussed earlier.

Figure 8 shows the influence of the radius R_2 on the biaxial stress - biaxial strain curve shape. In this case the radius R_1 was kept constant at 30 mm. From Figure 6 it is evident that as the radius R_2 increases from 10 to 30 mm, the biaxial stress decreases, and σ_b-ε_b curves tend to move down (in direction of the arrow) to lower values of biaxial stress. The decrease in biaxial stress with the increase in radius R_2 may be explained by the reason that the average dome thickness increases as the radius R_2 increases.

In order to evaluate the effect of R_1 and R_2 radii on the flow stress curve, a reference curve was introduced (Figs. 5 and 6). As shown in **Figures 7** and **8**, up to a biaxial strain of 0.3, all experimental curves are almost superimposed. The experimental stress-strain curves (up to a biaxial strain of 0.3) were fitted using the equations by Ghosh (G), Eq. (5), Hockett-Sherby (HS), Eq. (6), and a linear combination by Ghosh-Hockett-Sherby (GHS), Eq. (7), respectively.

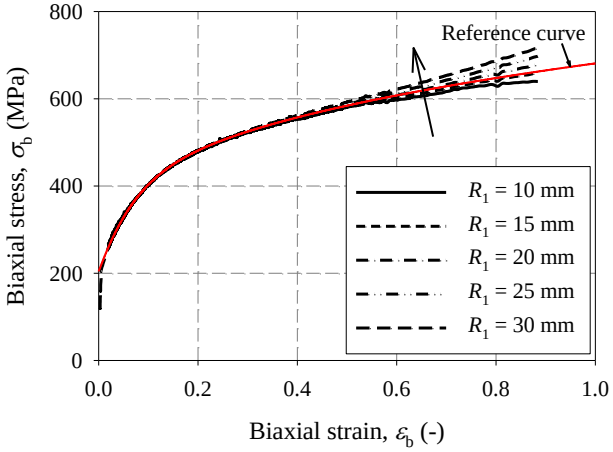

Figure 7. Effect of the radius R_1 on the biaxial stress - biaxial strain curve shape (R_2=5mm).

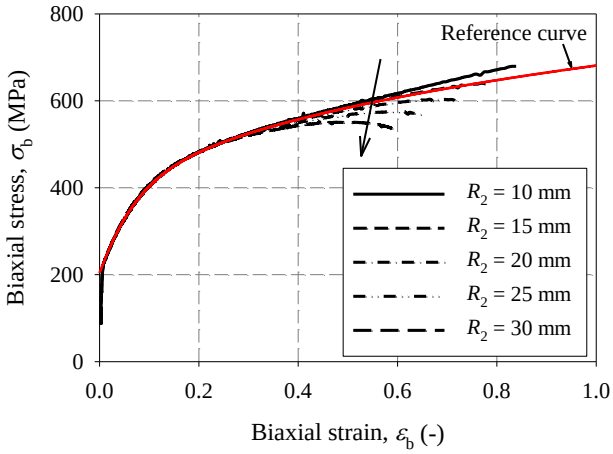

Figure 8. Effect of the radius R_2 on the biaxial stress - biaxial strain curve shape (R_1=30mm).

The Ghosh equation is given by

$$\sigma_y(G) = k(\varepsilon_0 + \varepsilon_p)^n - C\,, \tag{5}$$

and the Hockett-Sherby equation is

$$\sigma_y(HS) = A - (A-B)\exp(-m\cdot\varepsilon_p^n)\,. \tag{6}$$

The combination between Ghosh and Hockett-Sherby equation is

$$\sigma_y(GHS) = k\cdot\sigma_y(G) + (1-k)\cdot\sigma_y(HS)\,. \tag{7}$$

In Eqs. (1)-(3), ε_0 is initial plastic strain; n - hardening exponent, A, B, C, k and m -material constants.

In order to determine which of the three equations may sufficiently precise describe the experimental data, the statistical R-squared coefficient was used. The closer the value of R-squared to unity, the better the hardening law fit the experimental data. The result of fitting process is shown in **Figure 9**. The best fitting of experimental data was obtained using the equation by GHS, in which case the R-squared is 0.9994.

The curve given by GHS equation was plotted over the experimental curves in **Figures 7** and **8**. This curve called "reference curve" is used to asses the effect of R_1 an R_2 radii on the σ_b-ε_b curves. From **Figure 7** it is seen that the experimental curve obtained for R_1=15 mm and R_2= 5 mm (R_1/R_2=3), is in best agreement with the reference curve. In the same time, in **Figure 8**, the flow stress curve determined at R_1=30 mm and R_2= 15 mm (R_1/R_2=2), show the best agreement wit the reference curve. Therefore, in order to avoid the excessive shift up or down of flow stress curve, the ratio between R_1 an R_2 should be chosen between 2 and 3.

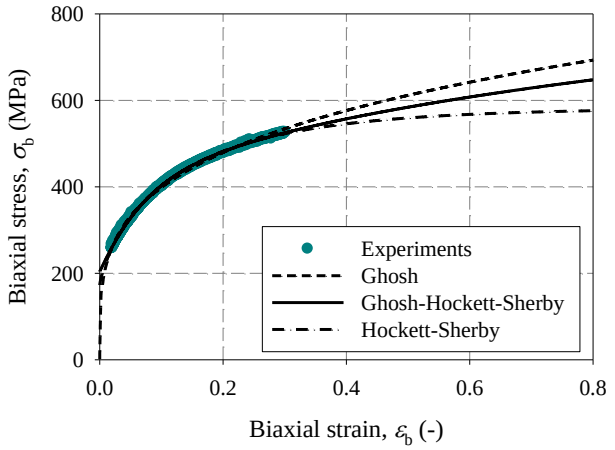

Figure 9. The fitted experimental data by using different hardening laws.

4. CONCLUSIONS

In this paper, the deviation of the specimen profile from its circular original profile has been investigated by Least Square Circle fitting of the experimental data at different bulge height. The effect of the procedural parameters (R_1) and (R_2) on the flow stress curve has been revealed using the ARAMIS software. Based on the obtained results, the following conclusions can be drawn:

1. The experimental meridian profile of specimen deviates from the assumed circle shape only when the bulge height is larger than 25 mm. The larger residuals were observed near the edges of the specimen, but the maximum value is under 0.4 mm.
2. The bulge radius increases when the radius (R_1) increases. At a bulge height of 32 mm, when the radius R_1 increases from 10 to 30 mm, the bulge radius increases with 5mm. This implicitly leads to the increasing in biaxial stress.
3. The biaxial stress increases when the radius (R_1) increases, and decreases when the radius (R_2) increases.
3. The experimental biaxial stress-biaxial strain curve is very close to the reference curve when the R_1/R_2 ratio is between 2 and 3.

5. REFERENCES

[1] A.J. Ranta-Eskola: Use of the hydraulic bulge test in biaxial tensile testing, Int. J. Mech. Sci. 21-8 (1979), 457–465.
[2] M. Atkinson: Accurate determination of biaxial stress-strain relationships from hydraulic bulging tests of sheet metals, Int. J. Mech. Sci. 39-7 (1996), 761-760
[3] D. Banabic, T. Bălan and D.S. Comsa, Closed-form solution for bulging through elliptical dies, J. Mater. Process. Tech. 115 (2001), 83-86.
[4] D. Banabic D., M. Vulcan, Bulge testing under constant and variable strain rates of superplastic aluminium alloys, Annales of CIRP, 54(2005), 205-209
[5] L. Lăzărescu, D.S. Comsa, D. Banabic, Analytical and experimental evaluation of the stress-strain curves of sheet metals by hydraulic bulge tests, Key Eng. Mat. 473 (2011) 352-359.
[6] A. Mutrux, B. Hochholdinger, P. Hora: A procedure for the evaluation and validation of the hydraulic biaxial experiments, Proc. Numisheet'08, ed. Hora P. Interlaken, Swish (2008), 67-71.
[7] M. Vucetic, A. Bouguecha, I. Peshekhodov, T. Götze, T. Huinink, H. Friebe, T. Möller, and B.-A. Behrens: Numerical Validation of Analytical Biaxial True Stress—True Strain Curves from the Bulge Test, Proc. NUMISHEET'11, eds. Chung K., Han H. N., Huh H., Barlat F., Lee M.-G., Seoul, Republic of Korea (2011), 107-114.
[8] X. Lemoine, S. Sriram, and R. Kergen: Flow Curve Determination at Large Plastic Strain Levels to Accurately Constitutive Equations of AHSS in Forming Simulation, Proc. ESAFORM'11, ed. Menary G., Belfast, United Kingdom (2011), 1417-1422.

Acknowledgements. This paper was supported by the projects: "Development and support of multidisciplinary postdoctoral programmes in major technical areas of national strategy of Research - Development - Innovation" 4D-POSTDOC, contract no. POSDRU/89/1.5/S/52603, POSDRU/107/1.5/S/78534 and PCCE 100/2010.